A Multiscale Computational Model Predicts Human Liver Function From Single-Cell Metabolism

König M.[1], Marchesini G.[2], Vilstrup H.[3], Somogyi A.[4] and Holzhütter HG.[1]

[1]Department of Computational Systems Biochemistry, University Medicine Charité Berlin, D-10117 Berlin, Germany
[2]Department of Internal Medicine, Aging and Nephrological Diseases, University of Bologna, I-40138 Bologna, Italy
[3]Department of Hepatology and Gastroenterology, Aarhus University Hospital, DK-8000 Aarhus, Denmark
[4]Biocomplexity Institute, Indiana University, Simon Hall MSB1, Bloomingtom, IN 47405

Running Title: Multiscale model of liver metabolism
Keywords: Virtual Liver, metabolism, liver, galactose, GEC

To whom correspondence should be addressed: Matthias König, Institute of Biochemistry, University Medicine Charité Berlin, Virchowweg 6, 10117 Berlin; Tel: (0049) 30450528197; Email: matthias.koenig@charite.de

ABSTRACT

Understanding how liver function arises from the complex interaction of morphology, perfusion, and metabolism from single cells up to the entire organ requires systems-levels computational approaches. We report a multiscale mathematical model of the Human liver comprising the scales from single hepatocytes, over representation of ultra-structure and micro-circulation in the hepatic tissue, up to the entire organ integrated with perfusion. The model was validated against data on multiple spatial and temporal scales. Herein we describe the model construction and application to hepatic galactose metabolism demonstrating its utility via i) the personalization of liver function tests based on galactose elimination capacity (GEC), ii) the explanation of changes in liver function with aging, and iii) the prediction of population variability in liver function based on variability in liver volume and perfusion. We conclude that physiology- and morphology-based multiscale models can improve the evaluation of individual liver function.

INTRODUCTION

The liver is the metabolic center of our body performing hundreds of functions including the homeostasis of numerous plasma metabolites; producing bile; detoxification of xenobiotics; and clearance of drugs and substances like galactose. In the past 30 years enormous progress in the knowledge and management of liver disease has been achieved, yet approximately 29 million people in the European Union still suffer from a chronic liver condition with underlying mechanism often being unclear {Blachier2013}. Liver function is the result of complex interplay of hepatic morphology, perfusion and metabolism across multiple spatial domains, from the cellular level up to the entire organ {Rappaport1979}. Computational models are uniquely positioned for the analysis of such complex systems and to capture the connectivity between these divergent scales and.

Liver Architecture

Liver architecture is unique in that it consists of a multitude of microscopic functional units termed lobules, which are connected in parallel to the blood flow. Within a single lobule a network of capillaries, the liver sinusoids transport the blood from the outer periportal regions, supplied via the portal vein and hepatic artery, to the central perivenous region, drained by the central vein {Sasse1992, Rappaport1979, Rappaport1973}. The sinusoidal unit, a single capillary perfused with blood and lined by a layer of hepatocytes forms the smallest functional unit of the liver (Figure 1) {Bass1977}. The fenestrated endothelial cells of the liver sinusoids act as a dynamic filter that permits exchange of fluid, solutes and particles between the sinusoidal lumen and space of Disse adjacent to the hepatocytes {Cogger2003}.

GEC as Liver function test

Quantification of liver function is necessary to assess the degree of liver impairment, to evaluate response to treatment and to select transplant recipients {Dufour1992}. Most function tests are based on the rate with which a given test substance is cleared specifically by the liver. Particularly, the liver is the primary organ for clearance and whole-body metabolism of galactose {Bernstein1960, Berry2000, Segal1971}. The determination of the maximal galactose removal rate, the galactose elimination capacity (GEC) {Marchesini1988, Schirmer1986, Tygstrup1966}, which is an established test of liver function measured in numerous studies {Jepsen2009, Fabbri1996}. Impairment of the liver in diseases like cirrhosis {Henderson1982, Jepsen2009} are associated with reduced GEC. Preoperative GEC predicts complications and survival after hepatic resection {Redaeli2002} and as predictor of survival in cirrhosis {Merkel1991, Salerno1996}.

The most extensive work on galactose elimination kinetics was done by Keiding and co-workers {} [43-45, 48, 50, 85, 99]. “These kinetic studies on the clearance of galactose at concentrations of 0 to 10 mg/dl (0 to 0.555 mmol/l) show that it approaches the ideal test substance for measuring effective liver blood flow (EHBF) (a) it is kinetically simple to analyse at steady state during continuous infusion (b) it is avidly removed by the liver, with minimal extrahepatic clearance and c) there is indirect evidence supporting virtually complete extraction by functional liver tissue on each pass.

Alterations in Aging

The percentage of deaths attributed to liver disease increases dramatically in humans beyond the age of 45 years {Schmucker2005}. In the elderly, a marked reduction in quantitative liver function measured by GEC {Schnegg1986, Marchesini1988} as well as major physiologic changes affecting liver function, i.e. decline in liver volume and blood flow {Anantharaju2002, Wynne1989, Marchesini1988}, are observed. In addition, characteristic changes in ultrastructure termed pseudocapillarization occur with aging, characterized by defenestration, thickening of the endothelium, and deposition of basal lamina and extracellular matrix in the space Disse {McLean2003, LeCouteur2001 , Cooger2003}. Age-related changes in the liver sinusoids are implicated in the association between ageing and impaired clearance of drugs {LeCouteur1998} and may provide a mechanistic link between primary aging processes and age-related disease {LeCouteur2002, Cogger2003}. Surprisingly, it is not clear to which extent age-inherent alterations in microangio-architecture, microvascular haemodynamics and liver volume and perfusion are contributing factors of age-related susceptibility of the liver {Vollmar2002}.

Multiscale-Model

Systems-level computational approaches are required to elucidate the complex interaction of organ structure, perfusion, and metabolism on multiple scales and to understand how these influence liver function, here the clearance of galactose and GEC. They are uniquely positioned to capture the connectivity between these divergent scales, as they can bridge the gap in understanding between isolated in vitro experiments and whole-organ in vivo models {Walpole2013}. Our objective was to develop such a multiscale computational model which i) describes physiology, morphology and function of the human liver; ii) can be applied to the evaluation of liver function tests, i.e. GEC; iii) can predict the effects of altered perfusion, liver volume and ultrastructure like occurring in aging on liver function; iv) can be integrated with patient data, and v) has clinical relevance.

RESULTS

We present a multiscale mathematical model of the human liver bridging the scales from individual cellular processes to the level of the entire organ. The model describes physiology, morphology and function of the human liver by integrating hepatic galactose metabolism with perfusion and liver structure (Figure 1). The model integrates and predicts experimental data on multiple temporal and spatial scales: i) prediction of hepatic multiple indicator dilution curves (Figure 2); iii) prediction of heterogeneity within sinusoids (hepatic zonation) and between sinusoids (Figure 2 and 3); prediction of galactose extraction, clearance and extraction fraction (Figure 4); iii) prediction of individual GEC, population variability in GEC and alterations in GEC with aging (Figure 4). We developed a classifier for liver disease based on our personalized model predictions for GEC outperforming regression approaches in a retrospective analysis of a large cohort study (Figure 4). We demonstrate possible clinical application of the presented systems biology approach by implementation of the classifier into a web application for simple use (Figure 5).

Multiscale Model of Human Liver

Our approach was … (independent units which could be tested, i.e. self consistent cell model,.. integration of scales & approaches)

Hepatocyte - Our model combines detailed kinetic models of cellular metabolism (Figure 1A) with a tissue-scale perfusion model of the sinusoid (Figure 1B). Despite the importance of the hepatic galactose metabolism for the systemic galactose clearance and formation of precursors for glycosylation reactions no detailed mathematical model of this pathway is available hitherto. This work presents to our knowledge the first kinetic model of galactose metabolism in hepatocytes (Figure 1A) comprising among others the three key enzymatic steps of galactose metabolization: i) the phosphorylation of galactose (gal) to galactose 1-phosphate (gal1p) catalysed by galactokinase (GALK, EC 2.7.1.6); ii) the conversion of gal1p to UDP-galactose (udpgal) by galactose-1-phosphate uridyl transferase (GALT, EC 2.7.7.10) and iii) the interconversion of udpgal and UDP-glucose (udpglc) by UDP-galactose 4´-epimerase (GALE, EC 5.1.3.2) {Novelli2000, Petry1998}. Galactose can enter glycolysis as glucose-1 phosphate (glc1p), one of the GALT reaction products, or can be incorporated as udpgal, the substrate donor of all galactosylation reactions, in glycoproteins and glycolipids {Novelli2000}.

Sinusoidal Unit - The cellular model is integrated into a realistic tissue-scale model of the sinusoidal liver unit based on known histological parameters (geometry, cell numbers, architecture, perfusion rates, …) (Figure 1C). Important features of liver architecture important for elimination, namely fenstraeted endothelial cells and space of Disse are explicitely represented in the model (see Methods).

Lobulus - Regional liver metabolism was modelled as weighted average across the heterogeneous contributions of tissue-scale models with differing in blood flow rates and tissue structure (Figure 1D, Figure 2A for parameter distributions). Similar to the classical distributed models of liver elimination {Bass1978}, but with an explicit description of ultrastructure and detailed kinetic models in the hepatocytes.

Mean sinusoidal unit & the integrated response over the heterogeneous contributions of sinusoids based on heterogeneity in ultra-structure and microcirculation are presented.

Liver anatomy ensures that periportal concentrations are common in all sinusoidal units. Outflow concentrations cv are assumed to be well mixed when they reach the hepatic vein.

Organ - Finally, the function of the entire organ is modelled by scaling of the regional output based on individual liver perfusion and liver volume, resulting in individualized liver function.

Personalization - Personalized multiscale models are generated based on individual anthropomorphic information in combination with fitted relationships describing the dependencies of hepatic volume and blood flow on these features.

Multiple Dilution-Indicator Curves

An indicator substances introduced into the blood flowing into the liver become dispersed in the effluent blood and the concentrations oft he substances in the effluent blood form an indicator dilution curve {Goresky1973}. The rapid injection of labeled red blood cells (a vascular indicator), labeled sucrose and albumin (extracellular references), and labeled galactose under various

galactose concentrations into the portal vein in combination with rapidly sampled venous blood were simulated {Goresky1973, Goresky1983} were simulated.

The model is a distributed model of flow based on parallel, non-interacting sinusoids joined at the venous terminus. The dispersion characteristics is due to the *a priori* incorporated experimental velocity and path length variations within the ensemble of sinusoids {Weiss1995}

In a first step the model was validated multiple-indicator dilution curves (Figure 2BC) {Goresky1973}. The single-injection, multiple-indicator dilution approach provides a method to determine the composition of the liver and the rates of hepatic processes {Goresky1973}. Labeled red blood cells (RBC) are used as vascular reference. Larger materials are excluded from the space of Disse. The outflow concentration of each tracer is divided by the total injected, providing a normalized value, an outflow fraction per ml. The integrated behavior based on molecular detailed description of single cell behavior give the correct multiple dilution indicator curves, consequently describing correctly the distribution of substances in the various spaces.
At low blood galactose concentrations, the labeled galactose appears at the outflow with labeled sucose, but is much reduced in magnitude, and exhibits a long tailing. Its outflow recovery is much reduced. At high blood galactose concentrations, the initial part of the profile increases towards that for labeled sucrose, the tailing becomes much larger in magnitude, and the outflow recovery becomes virtually complete {Goresky1973}. The shift of the dilution-indicator curves observed and explained by Goresky as different free volumes of the substances are a consequence of the different diffusion coefficients for the substances, and consequently altered distribution kinetics within the sinusoid and space of Disse resulting in a delayed appearance of the substances perivenous. None of the data was used for model fitting, all model parameters result from the geometric constraints of the system and the physiochemical properties of the substances transported within the sinusoid and the space of Disse. Only the exchange rates between hepatocytes and the space of Disse could be adapted, in the case of water freely, in case of galactose these fluxes are constrained by the total galactose elimination per volume tissue.

Heterogeneity between Sinusoids and within sinusoids

Our multiscale-model allows predictions about the cell to cell variability and the heterogeneity within the lobulus, i.e. between different sinusoidal units. By explicitly accounting for the observed heterogeneity in sinusoidal blood flow and ultrastructure (Figure 2A) we could analyze the local heterogeneity between different sinusoidal units in the tissue (Figure 2D). Due to the detailled modeling of the individual hepatocytes along the sinusoid the zonation patterns and gradients from periportal to perivenous could be analysed (Figure 3).
Individual cells within the sinusoid as well as different sinusoid show large differences in their time courses and local concentrations. Depending on local flow and morphology as well as location along the periportal-perivenous axis the acual concentration profiles are very heterogenous under identical periportal input concentrations.
Discuss, implications (Could explain the observed heterogeneity observed in NAFDL, locally

different concentrations, ...).
Discussion => not possible to reproduce dilution curves with single model with the correct Perfusion (i.e. mean perfusion). All single models completely underestimate the heterogeneity & are unable to reproduce dilution curves under physiological perfusion rates and volumes.

Hepatic Galactose Elimination

The extent to which blood flow or metabolic function determine the rate of clearance depends on the biochemical efficiency of the liver for removal of the substance relative to flow {Schirmer1986}. The effects of blood flow and substrate concentration on hepatic galactose elimination (GE), galactose clearance (CL), extraction ratio (ER) and perivenous concentrations were simulated (Figure 4A-H). The predictions are in excellent agreement with individual human data from multiple studies {Keiding1988, Tygstrup1958, Tygstrup1954, Waldstein1960, Henderson1982, Winkler1965, Palu1965} (Figure 4O-I).
The model predicts the Michaelis-Menten saturation kinetics of hepatic galactose elimination {Keiding1973, Keiding1976} with a concentration-dependent (first-order) elimination phase at low galactose concentrations and a definable clearance maximum, the galactose elimination capacity (GEC), at higher concentrations (zero-order phase) {Schirmer1986, Waldstein1960} (Figure4B). Three hepatic clearance regimes (flow-limited, general and enzyme-limited) can be defined {Winkler1978}:
i) In the enzyme-limited regime (gal > 6mM) the functional capacity, i.e. the galactose elimination capacity (GEC), can be evaluated via the rate of elimination at a sufficiently high galactose concentration where the elimination mechanisms are saturated {Winkler1978}. The clearance does not vary with the perfusion and is proportional to GEC {Winkler1979, Schirmer1986}. This is in line with the predicted constant arterio-hepatic venous concentration differences over a wide concentration interval (Figure 4H) supported by liver-vein catheterization studies {Tygstrup1954, Tygstrup1958}.
ii) In the flow limited clearance regime at low galactose concentrations (gal < 0.2mM) galactose clearance is a near ideal method for estimating the effective hepatic blood flow (EBHF) (Figure4A) {Schirmer1986}. The removal is completely determined by the perfusion (all substance removed in a single passage). The model predictions of near complete extraction of galactose across the liver with ER of around 0.9 at low galactose concentrations (Figure 4D) is in line with ER = 0.94 in subjects without hepatic disease by performing hepatic vein catheterization {Henderson1982}. Similar results were obtained by Keiding et al. with ER = 0.91±3 {Keiding1988}. The prediction of linear dependency of GE on perfusion for low galactose (Figure 4A) support this view.
ii) In the general galactose regime (0.2mM < gal < 6mM) blood flow as well as galactose concentration have strong influence on GE, CL and ER.
The model predicts lower galactose outflow concentrations under decreasing perfusion, in agreement with observed significantly lower outflow concentration during the period with low flow than during periods with high flow. {Keiding1978}.
The effects of pseudocapillarization with age were modeled and the respective curves simulated under the changed fenestraetion and endothelial cell sickness. Markly different galactose elimination and clearance is found under high perfusion and low galactose concentrations. This

can have important effects for
Depends strongly on the drug (albumin bound things are cleared much worse.

Metabolic effects

“In animals with saturated meatbolism (i.e. blood galactose concentrations > 2mmol/l), the liver concentrations are significantly increased in relation to the control animals for galactose-1-p, and UDP-galactose, and a significant reduction is seen for UDP-glucose, ATP and the sum of adenine nucleotides {Keiding1973, rat}.

Personalized GEC prediction

Reference ranges play an important role in clinical medicine, with values that lie outside the reference range viewed as an indication for further investigation and/or treatment {Cole2009}.
“The physiological variation in GEC (refs, Figure …) implies that it may be impossible to decide if the liver function is normal or not from a single determination of GEC, but if a reference value is obtainable, either in the same subject or in a comparable group, small variations in the liver function may be detectable {Tygstrup1964}".
We developed a method of estimating individual hepatic blood flow and liver volume from anthropomorphic information, i.e. age, gender, bodyweight, height and body surface area (BSA), based on predictive nonlinear models. Thereby it becomes possible to estimate the expected liver volume and liver blood flow for the given anthorpomorphic information and with this to calculate the expected clearance for the person. We employed this method to predict population variability in GEC. Of special interest were the changes in aging.
With estimated individual blood flows and liver volumes based on a comparable population sample the actual galactose elimination and especially the GEC can be predicted for individual subjects. ‘The mechanistic parameters, namely liver volume and hepatic blood flow were described with probability density functions (PDF) estimated from individual subject data (LMS, GAMLSS) approach. Since each PDF depicts the frequency of occurence of all expected values for each parameter in the population, the effects of multiple sources of uncertainty and variability were accounted for in the estimated distribution of GEC in the population.

- trainings sets

‘The significant correlation of GEC to BSA may indicate that the elimination capacity depends on the size of the liver (liver mass, Lm) {Tygstrup1964}

Predicted vs. experimental data points for liverVolumes, blood flows and GEC, GECkgare shown in Figure 5AB. (only data sets where at least the age was available were used as evaluation test set)

GEC in aging A significant negative correlation as observed between age and both liver volume and apparent liver blood flow above 30 years. The reduction in liver volume, apparent liver blood flow and perfusion may at least partly account for the decline in the clearance of many drugs undergoing liver metabolism, which has been noted to occur with aging in man {Wynne1989, Schnegg1986}. Also during childhood major absolute and relative changes per body weight occur in liver volume and bloodflow. To test if this underlying changes in liver morphology and perfusion can explain the age-dependent changes
Application of the model revealed that variability of galactose clearance in aging is mainly explained by changes in liver structure, perfusion and morphology during lifetime. These alterations with age have important implications for drug dosing.
TODO: discuss the effects of ultrastructur changes, only effects under low concentration clearance.

In infants and children younger than about 15 years, galactose is more rapidely eliminated than in adults {Tengström1968}
Red blood cell galactokinase activity was very low in erythrocytes of all elderly (>60 years) (24.4 +- 5.9 nmol/(min g hemoglobin) compared with young subjects (37.6 +- 4.5 nmol/(min g hemoglobin) {Birlouez-Aragon1992}

Population variability

Population Variability Given a cohort with anthropomorphic features for the the individuals our model allows the prediction of expected distribution of GEC values for the individuals in the cohort. If the cohort is representative for the population, the population variability of liver function can be estimated. We estimate the population variability in the US population based on the NHANES cohort {NHANES} (Figure 5BC). Not only GEC and GECkg are predictied correctly, but other pairwise correlations like the dependency of liver volume and blood flow from age, bodyweight, height and BSA (see Figures supplement). The presented methods allows thereby an estimation of the distribution of liver function based on the variability of hepatic perfusion and liver volume in the population.

Classification and Prediction of Liver Disease

We implemented a classifier for liver disease, i.e. cirrhosis, based on the multiscale model based prediction of individual liver function (GEC). The underlying idea was, that the further the experimental GEC of a subject deviates from the predicted GEC distribution based on their anthropomorphic information, the higher is the probability of impairment of the liver. We evaluated this approach retrospectively with data from a large cohort study (N=1012) {Fabbri1996} and additional data from the literature (N=112) {Ducry1979, duf1992, Marchesini1988, Schnegg1986, Tygstrup1963}. The classifier was evaluated against various logistic regression models on the same data sets {Figure 5E}. Classification based on our physiological multiscale model of the liver outperformed simple logistic regression models based on area under curve (AUC) and had similar performance to logistic regression with GEC, age and body weight as predictor. In contrast to the logistic regression, our classifier did not use the GEC data for training and is consequently applicable to different cohorts.

The prediction of personalized GEC ranges and subsequent classification of liver disease based on the presented multiscale-model was implemented in a web application (Figure 6). We hereby demonstrate the personalization of a multiscale-model of human liver with application to individualized evaluation of liver function tests.
This has important consequences for the evaluation of the functional capacity/reserve, the detection of impairments and disease, both crucial for organ evaluation in transplantation or in the calculation of proper drug dosage depending on age.
GEC as predictor in survival of cirrhosis {Merkel1991, Salerno1996} and detection of cirrhosis {Tygstrup1964}

Discussion

We have developed a multiscale. model that accounts for …

- explains a variety of emergent behaviors in terms of molecular interactions.
- *Our model accurately recapitulates a broad set of experimental data*
- *provides insights into several biological processes for which experimental assessment is not readily feasible, and enables ...*

mathematical modelling to make testable predictions and gain
insight about a biological system's behaviour.

The model includes the common key processes that lead to liver diseases, metabolism, perfusion and ultrastructure of the liver. The multiscale model's explicitly modeled tires of resolution provide information beyond that which can be obtained by independently exploring single scales in isolation.

A clear and immediate need exists for evidence-based guidance for the identification of people being at risk of liver disease, and follow-up in deteriotation / improvement of liver function.

Model assumptions

A mathematical model is always only a selective representation of reality. Certain model assumption had to be made due to lack of data and the boundaries of the model

- We could not retrieve correlation data between sinusoidal blood flows and ultrastructural parameters of the liver. The distributions of sinusoidal parameters were assumed statistically independent from each other.
- No changes in gene expression, protein levels were taken into account. Galactose metabolism and GEC are quit constant. Adult rats fed a 40% galactose diet for 5 days did not show an increase in GEC although 20 days on the diet resulted in a 20% increase in V_{max} suggesting that adaptive mechanisms are slow [Schirmer1986 ->18]. This lack of inducability and relatively constant V_{max} is desirable in clearance methodology as a fluctuating V_{max}/FK_m would certainly complicate clearance interpretations. An important part of the individual GEC is the actual protein expression of the key enzymes. With the availablity of omics data these can readily be integrated in the model to further improve

personalized predictions of elimination rates.
Results from rats fed low protein diets indicate that GEC in rats deprieved of dietary protein is determined by the amount of hepatic protein. GEC was signifcantly decreased to appoximately half of control values with hepatic protein content reduced to the same extent {Vilstrup1976}

- Dispersion of dilution peaks in the large vessels and runtime differences were not modelled. It is assumed that no displacement occurs between reference intravascular and diffusible tracers in the large vessels: all displacement occurs in the exchanging vessels (sinusoids). The interrelations between whole-organ outflow reference and diffusible tracer curves will depend not only on the phenomena occurring within each sinusoid but also on the way the transit times in larger vessels and sinusoids are interrelated. Various combinations are possible, depending on the structure of the network and the kind of flow coupling in the system. The pattern corresponding to the liver was found to lie at a simple extreme in this possible spectrum [Rose1976, Goresky1970]. The distribution of out-flow transit times was found to correspond to the distribution transit of sinusoidal times in large transit times; the distribution of vessels was so compact that a single value could be assumed [Rose1976, Goresky1970] supporting the model assumption.
- The other question is if heterogeneity in sinusoidal blood flow and transit times exist. Goresky et al.1 previously have considered two models representing the extreme cases, i.e., no heterogeneity, and maximum heterogeneity in capillary transit times. Multiple indicator-dilution data from the liver fit the latter model well [Rose1976].
- Heterogeneity in local blood flow in the liver was not taken into account.
- f_flow=0.5 => Factor 2 in Via the relationship for normal perfusion of 1.2ml/min/ml an necessary adaption of the microcirculation of f_{flow}=0.3 results corresponding to a mean sinusoidal flow velocity of 81µm/s. This is still in the range of the experimentally obtained values. OPS values and microcirculation is taken on the surface of the liver, with partly larger arterial components and properly not representative of the whole liver.

- Part of the model relies on predictive models of liver volume and bloodflow which were trained with trainingssets based on multiple studies. The predictions reflect this subset of data used for model fitting. Care was taken only to use data for Caucasian/Western individuals with normal bodyweight range and without any liver disease. Nonetheless the regression models reflect the used trainingssets.

Most of these assumptions are necessary to a lack of experimental data or the focus of the current modeling question. We see this model as a first draft. The model and all source code is made freely available under xxx licence and is available from.

Comparison to other liver models

- Höhme (no detailed blood flow & heterogeneity, no metabolism, based on rat data, no space of Disse, fenestraetion, no evaluation against multiple indicator data & at same time total rates)

- Chaloubh & other simple sinusoid models without flow heterogeneity (missing parameter distributions, only briding the gap to the sinusoidal unit, not possible to simulate the different effects of heterogenous variations of parameters, no scaling to liver)
  These models do not reflect the reality of highly heterogeneous bloodflow and liver on sinusoidal scale.
- Distributed models, simple clearance models (Bass, Keiding, …) -> no detailed metabolism, can not answer the effects on cell level (good approximations for many cases)
- Ricken & other porous media approaches (human cast model!) (only on lobulus level, no modeling of actual ultrastructure, different approach for different questions, material-properties, stiffness)

All models fail in accounting … & and none could demonstrate clinical relevance.

Classifier

The here presented classifier has the large advantage of independence of cohort data. Constructed based on underlying physiological principles, i.e. how is the liver architecture, how is galactose metabolized and how are the observed liver volumes and blood flows in the population. No overfitting to cohort data, and direct interpretation of the parameters. Provides platform for testing hypothesis for liver function and disease mechanisms.
No fitting to prediction data, but independent development.
=> wide applicability

Transfer to other substances

In case of the GEC the liver volume is the deterimening factor under high galactose concentrations. For other eliminated compounds and drugs flow could be important (depending on the actual clearance regime of the substance in question). The provided modeling framework allows a straight-forward transfer to the hepatic elimination of other drugs. The only drug specific component are the metabolic networks within the hepatocytes. The complete infrastructure can be readily applied to other questions like BSP, ICG, drug clearance, ...

Significance

drug dosing & timing
“The capacity of the liver to eliminate various substances from the blood is important clinically. The elimination of several drugs depends on liver function, and correct dosage presumes information on their hepatic elimination kinetics. {Keiding1976}”

Clearance of substances & liver functions

It can be challenging to design tests of liver functions based on measurement of Vmax at high blood concentration in man, due to toxicity or unwanted haemodynamic or osmotic effects or the costs for large amounts of test substance {Winkler1978}. Our model provides means to calculate the complex interactions between perfusion and metabolism in the various elimination regimes and can evaluate also the cases where flow has a strong effect on clearance, i.e. not necessary to work in the Vmax regime.

Towards a virtual liver & future applications

Bridging the scales from cellular processes over the coupling of single cells within the tissue-architecture towards whole-organ models is a crucial step in understand physiological function of organs in the normal state and in pathophysiologies. Only by modelling the different scales explicitly the emerging behaviour on a liver scale can be properly understood.

- the systems biology approach, i.e. the interaction between biological experiments and mathematical modelling, is to be transferred to application-oriented liver research as a next step
- In order to use the understanding of these processes to develop novel treatment and prevention approaches, disease-relevant and, if possible, personalized multiscale models are to be derived.

ACKNOWLEDGEMENT

This work was supported by the Federal Ministry of Education and Research (BMBF, Germany) within the Virtual Liver Network (VLN grant number 0315741). We want to thank H. Wynne {Wynne1989}, A. Heinemann {Heinemann1999}, G. Cattermole {Cattermole2010} for access to original publication data, SABIO-RK for integration of kinetic parameters, in particular M. Golebiewski, R. Kenia and U. Wittig, T. Czauderna for help with SBGN and SBGN-ED {Czauderna2010} and the SBML community for their continuous support and help.
The authors declare no commercial or financial conflict of interest.
All source code, model data and results are freely available https://github.com/matthiaskoenig/multiscale-galactose).

REFERENCES

Anantharaju, Abhinandana, Axel Feller, and Antonio Chedid. "Aging liver." *Gerontology* 48.6 (2002): 343-353.
Bass, L, P Robinson, and AJ Bracken. "Hepatic elimination of flowing substrates: the distributed model." *Journal of theoretical biology* 72.1 (1978): 161-184.
Bernstein, L.M., et al. (1960) The blood galactose disappearance curve as a test of liver function, Gastroenterology, 39, 293-304.
Berry, G.T., et al. (2000) Galactose breath testing distinguishes variant and severe galactose-1-phosphate uridyltransferase genotypes, Pediatric research, 48, 323-328.
Birlouez-Aragon, I., Ravelontseheno, L., Villate-Cathelineau, B., Cathelineau, G., & Abitbol, G. (1993). Disturbed galactose metabolism in elderly and diabetic humans is associated with cataract formation. *The Journal of nutrition*, *123*(8), 1370-1376.
Blachier, M., Leleu, H., Peck-Radosavljevic, M., Valla, D., & Roudot-Thoraval, F. (2013). The burden of liver disease in Europe: a review of available epidemiological data. *Journal of hepatology*, *58*(3), 593-608.
Bosch, A.M., et al. (2002) Clinical features of galactokinase deficiency: a review of the literature, Journal of inherited metabolic disease, 25, 629-634.
Cattermole, Giles N et al. "The normal ranges of cardiovascular parameters in children measured using the Ultrasonic Cardiac Output Monitor." *Critical care medicine* 38.9 (2010): 1875-1881.
Centers for Disease Control and Prevention (CDC). National Center for Health Statistics (NCHS). National Health and Nutrition Examination Survey Data (NHANES). Hyattsville, MD: U.S. Department of Health and Human Services, Centers for Disease Control and Prevention, 1999-2012, http://www.cdc.gov/nchs/nhanes/nhanes_questionnaires.htm.
Cogger, Victoria C et al. "Hepatic sinusoidal pseudocapillarization with aging in the non-human primate." *Experimental gerontology* 38.10 (2003): 1101-1107.
Cole, Timothy J, and Pamela J Green. "Smoothing reference centile curves: the LMS method and penalized likelihood." *Statistics in*

medicine 11.10 (1992): 1305-1319.
Czauderna, T., Klukas, C. and Schreiber, F. (2010) Editing, validating and translating of SBGN maps, Bioinformatics, 26, 2340-2341.
Dufour, J., Stoupis, C., Lazeyras, F., Vock, P., Terrier, F., & Reichen, J. (1992). Alterations in hepatic fructose metabolism in cirrhotic patients demonstrated by dynamic 31phosphorus spectroscopy. *Hepatology*, *15*(5), 835-842.
Fabbri, A., Bianchi, G., Motta, E., Brizi, M., Zoli, M., & Marchesini, G. (1996). The galactose elimination capacity test: a study of the technique based on the analysis of 868 measurements. *The American journal of gastroenterology*, *91*(5), 991-996.
Fridovich-Keil, J.L. (2006) Galactosemia: the good, the bad, and the unknown, Journal of cellular physiology, 209, 701-705.
Goresky, C.A., Bach, G.G. and Nadeau, B.E. (1973) On the uptake of materials by the intact liver. The transport and net removal of galactose, The Journal of clinical investigation, 52, 991-1009.
Goresky, C. A. (1983). Kinetic interpretation of hepatic multiple-indicator dilution studies. *Am. J. Physiol*, *245*(1), G1-12.
Heinemann, Axel et al. "Standard liver volume in the Caucasian population." *Liver transplantation and surgery* 5.5 (1999): 366-368.
Henderson, J.M., Kutner, M.H. and Bain, R.P. (1982) First-order clearance of plasma galactose: the effect of liver disease, Gastroenterology, 83, 1090-1096.
Jepsen, P., et al. (2009) The galactose elimination capacity and mortality in 781 Danish patients with newly-diagnosed liver cirrhosis: a cohort study, BMC gastroenterology, 9, 50.
Keiding, S. (1973). Galactose elimination capacity in the rat. *Scandinavian Journal of Clinical & Laboratory Investigation*, *31*(3), 319-325.
Keiding, S., Johansen, S., Winkler, K., Tonnesen, K., & Tygstrup, N. (1976). Michaelis-Menten kinetics of galactose elimination by the isolated perfused pig liver. *American Journal of Physiology--Legacy Content*, *230*(5), 1302-1313.
Keiding, S. (1988). Gatactose Eiearance Measurements and Liver Blood Flow. *Gastroenterology*, *94*(2), 477-81.
Keppler, D., Rudigier, J. and Decker, K. (1970) Trapping of uridine phosphates by D-galactose in ethanol-treated liver, FEBS letters, 11, 193-196.
Knop, J.K. and Hansen, R.G. (1970) Uridine diphosphate glucose pyrophosphorylase. IV. Crystallization and properties of the enzyme from human liver, The Journal of biological chemistry, 245, 2499-2504.
Konig, M., Holzhutter, H.G. and Berndt, N. (2013) Metabolic gradients as key regulators in zonation of tumor energy metabolism: A tissue-scale model-based study, Biotechnology journal, 8, 1058-1069.
Le Couteur, D. G., Fraser, R., Cogger, V. C., & McLean, A. J. (2002). Hepatic pseudocapillarisation and atherosclerosis in ageing. *The Lancet*, *359*(9317), 1612-1615.
Le Novere, N., et al. (2009) The Systems Biology Graphical Notation, Nature biotechnology, 27, 735-741.
Leslie, N.D. (2003) Insights into the pathogenesis of galactosemia, Annual review of nutrition, 23, 59-80.
Marchesini, G., et al. (1988) Galactose elimination capacity and liver volume in aging man, Hepatology, 8, 1079-1083.
Merkel, C., Gatta, A., Zoli, M., Bolognesi, M., Angeli, P., Iervese, T., et al. (1991). Prognostic value of galactose elimination capacity, aminopyrine breath test, and ICG clearance in patients with cirrhosis. *Digestive diseases and sciences*, *36*(9), 1197-1203.
McLean, Allan J et al. "Age - related pseudocapillarization of the human liver." *The Journal of pathology* 200.1 (2003): 112-117.
Mosteller, RD. "Simplified calculation of body-surface area." *The New England journal of medicine* 317.17 (1987): 1098.
Novelli, G. and Reichardt, J.K. (2000) Molecular basis of disorders of human galactose metabolism: past, present, and future, Molecular genetics and metabolism, 71, 62-65.
Dal Palù, C., Spandri, P., & Zuin, R. (1965). Hepatic Clearance and Lm of Galactose in Normal and Cirrhotic Subjects. *Postgraduate medical journal*, *41*(475), 261.
Pappenheimer, J. R. (1953). Passage of molecules through capillary walls. *Physiol. Rev*, *33*(3), 387-423.
Petry, K.G. and Reichardt, J.K. (1998) The fundamental importance of human galactose metabolism: lessons from genetics and biochemistry, Trends in genetics : TIG, 14, 98-102.
Rappaport, AM. "The microcirculatory hepatic unit." *Microvascular research* 6.2 (1973): 212-228.
Rappaport, AM. "Hepatic blood flow: morphologic aspects and physiologic regulation." *International review of physiology* 21 (1979): 1-63.
Renkin, E. M. (1954). Filtration, diffusion, and molecular sieving through porous cellulose membranes. *The Journal of general physiology*, *38*(2), 225-243.
Redaelli, C. A., Dufour, J., Wagner, M., Schilling, M., Hüsler, J., Krähenbühl, L., et al. (2002). Preoperative galactose elimination capacity predicts complications and survival after hepatic resection. *Annals of surgery*, *235*(1), 77.
Salerno, F., Borroni, G., Moser, P., Sangiovanni, A., Almasio, P., Budillon, G., et al. (1996). Prognostic value of the galactose test in predicting survival of patients with cirrhosis evaluated for liver transplantation: A prospective multicenter italian study. *Journal of hepatology*, *25*(4), 474-480.
Sasse, D., Spornitz, U.M. and Maly, I.P. (1992) Liver architecture, Enzyme, 46, 8-32.
Schadewaldt, P., et al. (2000) Analysis of concentration and (13)C enrichment of D-galactose in human plasma, Clinical chemistry, 46, 612-619.
Schirmer, W.J., et al. (1986) Galactose clearance as an estimate of effective hepatic blood flow: validation and limitations, The Journal of surgical research, 41, 543-556.

Schmucker, Douglas L. "Age-related changes in liver structure and function: implications for disease?." *Experimental gerontology* 40.8 (2005): 650-659.
Schnegg, Marianne, and Bernhard H Lauterburg. "Quantitative liver function in the elderly assessed by galactose elimination capacity, aminopyrine demethylation and caffeine clearance." *Journal of hepatology* 3.2 (1986): 164-171.
Segal, S. and Rogers, S. (1971) Nucleotide inhibition of mammalian liver galactose-I-phosphate uridylyltransferase, Biochimica et biophysica acta, 250, 351-360.
Somogyi, Andi, Simulation of electrochemical and stochastic systems using just in time compiled declarative languages, doctoral thesis (2014)
Somogyi, E.T et al., (2015), libRoadRunner: A High Performance SBML Simulation and Analysis Package, submitted
Stasinopoulos, D Mikis, and Robert A Rigby. "Generalized additive models for location scale and shape (GAMLSS) in R." *Journal of Statistical Software* 23.7 (2007): 1-46.
Tang, M., et al. (2012) Correlation assessment among clinical phenotypes, expression analysis and molecular modeling of 14 novel variations in the human galactose-1-phosphate uridylyltransferase gene, Human mutation, 33, 1107-1115.
Timson, D.J. (2005) Functional analysis of disease-causing mutations in human UDP-galactose 4-epimerase, The FEBS journal, 272, 6170-6177.
Timson, D.J. and Reece, R.J. (2003) Functional analysis of disease-causing mutations in human galactokinase, European journal of biochemistry / FEBS, 270, 1767-1774.
Timson, D.J. and Reece, R.J. (2003) Sugar recognition by human galactokinase, BMC biochemistry, 4, 16.
Tyfield, L. and Walter, J. (2002) Galactosemia. In Scriver, C., et al. (eds), The Metabolic and Molecular Bases of Inherited Disease. McGraw-Hill, New York.
TYGSTRUP, N., & WINKLER, K. (1954). Kinetics of galactose elimination. *Acta Physiologica Scandinavica*, *32*(4), 354-362.
TYGSTRUP, N. (1964). The galactose elimination capacity in control subjects and in patients with cirrhosis of the liver. *Acta Medica Scandinavica*, *175*(3), 281-289.
Tygstrup, N., & Winkler, K. (1958). Galactose blood clearance as a measure of hepatic blood flow. *Clinical science (London, England: 1979)*, *17*(1), 1-9.
Tygstrup, N. (1966) Determination of the hepatic elimination capacity (Lm) of galactose by single injection, Scandinavian journal of clinical and laboratory investigation. Supplementum, 18, 118-125.
Vollmar, Brigitte et al. "In vivo quantification of ageing changes in the rat liver from early juvenile to senescent life." *Liver* 22.4 (2002): 330-341.
Villeneuve, J.P., et al. (1996) The hepatic microcirculation in the isolated perfused human liver, Hepatology, 23, 24-31.
Vilstrup, H. (1983) Effects of acute carbon tetrachloride intoxication on kinetics of galactose elimination by perfused rat livers, Scandinavian journal of clinical and laboratory investigation, 43, 127-131.
Waldstein, S. S., Greenburg, L. A., Biggs Jr, A., & Corn, L. (1960). Demonstration of hepatic maximum removal capacity (Lm) for galactose in humans. *Journal of Laboratory and Clinical Medicine*, *55*, 462-475.
Walter, J.H., et al. (1999) Generalised uridine diphosphate galactose-4-epimerase deficiency, Archives of disease in childhood, 80, 374-376.
Walpole, Joseph, Jason A Papin, and Shayn M Peirce. "Multiscale computational models of complex biological systems." *Annual review of biomedical engineering* 15 (2013): 137.
Weiss, M. (1997). A note on the interpretation of tracer dispersion in the liver. *Journal of theoretical biology*, *184*(1), 1-6.
Winkler, K., Larsen, J., Munkner, T., & Tygstrup, N. (1965). Determination of the hepatic blood flow in man by simultaneous use of five test substances measured in two parts of the liver. *Scandinavian Journal of Clinical & Laboratory Investigation*, *17*(5), 423-432.
Winkler, K., Bass, L., Keiding, S., & Tygstrup, N. (1978). The physiologic basis for clearance measurements in hepatology. *Scandinavian journal of gastroenterology*, *14*(4), 439-448.
Wisse, E., et al. (1985) The liver sieve: considerations concerning the structure and function of endothelial fenestrae, the sinusoidal wall and the space of Disse, Hepatology, 5, 683-692.
Wittig, U., et al. (2012) SABIO-RK--database for biochemical reaction kinetics, Nucleic Acids Res, 40, D790-796.
Wynne, Hilary A et al. "The effect of age upon liver volume and apparent liver blood flow in healthy man." *Hepatology* 9.2 (1989): 297-301.

Online Methods

The presented liver model is a multi-scale model comprising the metabolism of individual hepatocytes on cellular scale (Figure 1A), the individual sinusoidal unit on tissue scale (Figure 1B), the representation of lobulus via integration of multiple sinusoidal units (Figure 1C), the representation of the individual liver based on correlations between liver volume and blood flow and anthropomorphic features up to the variability in the population based on observed combination of anthropomorphic features in the population (Figure 1D).

Availability of data and models

All code and models and literature based datasets are made freely available. The cellular and sinuosoidal unit model are provided as SBML under creative commons (CC BY-SA 4.0) in the supplement and on Biomodels.org and JWS Online. A human-readable HTML representation of the model is provided in the supplement.

Numerical integration

The single hepatocyte and models of sinusoidal units are ordinary differential equation (ODE) based kinetic models. The models were integrated with libRoadRunner v1.3 {Somogyi2014, Somogyi2015} with absolute and relative tolerances of 1E-6. LibRoadRunner was further developed to efficiently handle very large SBML models via ...
All simulations and time courses were stored in a database.

Cellular scale - galactose metabolism

The kinetic model of galactose metabolism for individual hepatocytes consists of three main enzymatic steps i) the phosphorylation of galactose (gal) to galactose 1-phosphate (gal1p) catalysed by galactokinase (GALK, EC 2.7.1.6); ii) the conversion of gal1p to UDP-galactose (udpgal) by galactose-1-phosphate uridyl transferase (GALT, EC 2.7.7.10) and iii) the interconversion of udpgal and UDP-glucose (udpglc) by UDP-galactose 4´-epimerase (GALE, EC 5.1.3.2) {Novelli2000, Petry1998}. Galactose can enter glycolysis as glucose-1 phosphate (glc1p), one of the GALT reaction products, or can be incorporated as udpgal, the substrate donor of all galactosylation reactions, in glycoproteins and glycolipids {Novelli2000}. The alternative processes important in galactosemias and ATP synthesis (ATPS) and NADP reduction (NADPR) for cofactor regeneration were added to the model. Detailed information on metabolites, initial concentrations, rate equations and enzymatic parameters is provided in Supplementary Table 1 and Supplementary Table 2. The literature based kinetic parameters were included in SABIO-RK {Wittig2012} and annotated in the model (see Supplementary Tables and SBML annotations). Maximal enzyme activities (V_{max}) were chosen to achieve good correspondence of model simulations with reported galactose elimination rates in young subjects (20 years).

Sinusoidal Unit

The tissue-scale model of the sinusoidal unit (Figure 1B) consists of a central blood vessel (sinusoid) surrounded by the space of Disse and adjacent hepatocytes in cylindrical geometry

with parameters in Supplementary Table 3 and Supplementary Table 4. The periportal (pp) and perivenous (pv) blood compartments are located adjacent to the first and last sinusoidal volume, respectively. A single sinusoidal unit consists of N_c hepatocytes with each cell having a single associated sinusoid and Disse volume. In the sinusoid substances are transported by blood flow and diffusion, in the space of Disse solely by diffusion. Red blood cells (RBC) are constricted to the sinusoid, whereas all other model substances smaller than the fenestrae ($r_{substance} \leq r_{fen}$) pass in the space of Disse owing to the fenestration of the endothelial cells {Wisse1985}, i.e. galactose, albumin, sucrose and water. Galactose and water are exchanged between the space of Disse and the hepatocytes, whereas sucrose and albumin are restricted to the space of Disse.

Diffusion and blood flow are modelled via discretized one-dimensional diffusion and convection equations (analogue to {Konig2013}). The diffusion through the sinusoidal fenestration, small cylindrical channels in the endothelial cells is described via pore theory {Pappenheimer1953, Renkin1954}. The total restriction to diffusion due to the combined effects of steric hindrance at the entrance of the pores and frictional resistance within the pores for substance a with radius r_a is given as actual diffusion D_a relative to unhindered Diffusion $D_{a,0}$ with radius of the substance r_a and pore radius r_{fen} as

$$\frac{D_a}{D_{a,0}} = (1 - \frac{r_a}{r_{fen}})^2 \left[1 - 2.104(\frac{r_a}{r_{fen}}) + 2.09(\frac{r_a}{r_{fen}})^3 - 0.95(\frac{r_a}{r_{fen}})^5\right]$$ {Renkin1954}.

Heterogeneity of Sinusoidal Units

The heterogeneity of sinusoidal units within a lobulus was modeled via a Monte Carlo approach simulating a multitude of heterogeneous sinusoidal units based on experimental parameter distributions (Figure 2) for the the ultrastructure (sinusoidal length L_{sin}, sinusoidal radius y_{sin}, width space of Disse y_{dis}, hepatocyte sheet thickness y_{cell}) and microcirculation (sinusoidal blood flow velocity v_{blood}). The output of the lobulus is calculated as the integrated response over all sinusoidal unit samples in the region of interest (N_{sin}=1000). The parameter distributions were assumed log-normal and statistically independent of each other. Distributions of y_{sin}, v_{blood} and y_{cell} were fitted based on maximum-likelihood method for uni-variate distributions. For L_{sin} and y_{dis} the log-normal parameters were calculated from reported mean m and standard deviation std. The resulting distribution parameters and experimental data are given in Supplementary Table 4.

Variation in perfusion is modeled by scaling the distribution of sinusoidal blood flows $p(v_{blood})$ via $p_{f=f_{flow}}(v_{blood}) = p(f_{flow} v_{blood})$ to higher or lower blood flows with $p_{f=1}$ corresponding to the experimental microcirculation.

Integration of Sinusoidal Units (Lobulus)

To calculate the response of a lobulus the simulation results of N_{sin} sinusoidal units under identical periportal boundary conditions are integrated, each sampled from the parameter distributions corresponding to the simulated conditions. For instance the lobulus perfusion is

calculated from the volumes V[k] and blood flows Q[k] for individual sinusoidal with $x_{tot} = \sum_{k=1}^{N_{sin}} x[k]$ and $< x > = \frac{1}{N_{sin}} \sum_{k=1}^{N_{sin}} x[k]$ as $P_{sin} = \frac{Q_{sintot}}{V_{sintot}} = \frac{\sum_{k=1}^{N_{sin}} Q_{sin}[k]}{\sum_{k=1}^{N_{sin}} V_{sin}[k]}$

This integration over the sinusoidal units only accounts for the parenchymal fraction of the liver volume of around 80% (f_{tissue}=0.8). Accounting for the non parenchymal volume of the liver, consisting mainly of large vessel volume the tiss volume V_{tissue} is calculated from the sinusoidal liver volume V_{sin} as

$V_{tissue} = V_{sin} + V_{ves} = (2 - f_{tissue}) V_{sin}$

resulting in the tissue perfusion

$P_{tissue} = \frac{Q_{sintot}}{V_{tissue}} = \frac{1}{(2-f_{tissue})} \frac{Q_{sintot}}{V_{sintot}}$

The integration of tissue galactose elimination and clearance is performed in an analogue way.

Multiple Indicator Dilution Curves

The multiple indicator dilution curves under varying unlabeled galactose concentration were modeled via: i) running simulation to steady state under given unlabeled galactose concentration; ii) giving a periportal tracer peak of duration 0.5s. The hepatic vein tracer concentration for substance s is calculated as flow weighted average of the perivenous time courses of the individual sinusoidal units $c_{pv}^{s}[k]$, i.e.

$$c_{ven}^{s}(t) = \sum_{k=1}^{N_{sin}} w_k c_{pv}^{s}[k](t) = \sum_{k=1}^{N_{sin}} \frac{Q_{sin}[k]}{Q_{sintot}} c_{pv}^{s}[k](t)$$

For the comparison with experimental data the catheter and nonexchangeable vessel transit time t_0 were estimated from the time of first appearance of radioactivity above background levels in the experimental and simulated dilution curves. This zero point was used for mapping simulations and experiments. The dilution curves are simulated with reported GEC values for dogs of ~ 0.5 * GEC of humans (see supplement).

Galactose Elimination, Extraction Ratio and Clearance

The galactose elimination rate (GE), extraction ratio (ER) and clearance (CL) for a single sinusoidal unit k are calculated from sinusoidal blood flow Q_{sin}[k] and periportal and perivenous galactose concentrations $c_{pp}^{gal}[k]$ and $c_{pv}^{gal}[k]$ in steady state {Schirmer1986}

$$GE[k] = Q_{sin}[k](c_{pp}^{gal}[k] - c_{pv}^{gal}[k])$$

$$ER[k] = \frac{c_{pp}^{gal}[k] - c_{pv}^{gal}[k]}{c_{pp}^{gal}[k]}$$

$$CL[k] = Q_{sin}[k] \frac{c_{pp}^{gal}[k] - c_{pv}^{gal}[k]}{c_{pp}^{gal}[k]} = Q_{sin}[k]\, ER[k]$$

The integrated GE, ER and CL per tissue volume liver for N_{sin} sinusoidal units, are calculated with the volume of the individual sinusoidal units V[k] as

$$GE_{tissue} = \frac{1}{(2-f_{tissue})} \frac{Q_{sintot}}{V_{sintot}} < c_{pp}^{gal}[k] - c_{pv}^{gal}[k] >= P_{tissue} < c_{pp}^{gal}[k] - c_{pv}^{gal}[k] >$$

$$ER_{tissue} =< \frac{c_{pp}^{gal}[k] - c_{pv}^{gal}[k]}{c_{pp}^{gal}[k]} >$$

$$CL_{tissue} = \frac{1}{(2-f_{tissue})} \frac{Q_{sintot}}{V_{sintot}} < \frac{c_{pp}^{gal}[k] - c_{pv}^{gal}[k]}{c_{pp}^{gal}[k]} >= P_{tissue} < \frac{c_{pp}^{gal}[k] - c_{pv}^{gal}[k]}{c_{pp}^{gal}[k]} >$$

Clearance based on equilibrium galactose concentrations overestimate hepatic clearance of galactose especially at very low galactose concentration due to small basal systemic galactose clearance R_{base} outside kidney and liver as reported by {Keiding1988} and discussed in {Waldstein1960}. Consequently, the experimental data for ER and CL {Tygstrup1958, Tygstrup1954, Waldstein1960, Henderson1982, Winkler1965, Palu1965} was corrected for R_{base} with V_{max}^{R} =0.114 [mmol/min] fitted with the data from {Keiding1988} and K_m^R = 0.2 mM in the range of galactokinase Km for galactose. The correction calculates depending on the equilibrium galactose concentration gal_{eq} the respective systemic basal clearance

$$R_{base}(gal_{eq}) = V_{max}^{R}(\frac{gal_{eq}}{gal_{eq} + K_m^R})$$

giving corrected experimental clearance and galactose elimination as

$$GE_{liver} = GE_{exp} - R_{base}$$

and

$$CL_{liver} = CL_{exp} - \frac{R_{base}}{gal_{eq}}$$

Extrahepatic, intracorporeal removal of galactose is likely. In animals which have undergone hepatectomy, nephrectomy and evisceration, galactose disappears from the blood although at a slow rate [17]. Studies in which radioactive C14 galactose has been used have demonstrated metabolism of galactose by tissues other than the liver [18]. One explanation => is small but constant amount of extrahepatic removal. The estimated maximal systemic GEC is ~4% of the hepatic GEC.

For comparison with the experimental data the per tissue model predictions were scaled to the complete liver under assumption of V_{liver}=1500ml resulting in blood flow $Q_{liver} = P_{tissue}V_{liver}$, galactose elimination $GE_{liver} = GE_{tissue}V_{liver}$ and clearance $CL_{liver} = CL_{tissue}V_{liver}$.

Alterations in aging

Changes in ultrastructure of the liver (pseudocapillarization) were modeled via decreasing the parameters for fenestration number per area (N_{fen}), and increasing the endothelial thickness (y_{end}) with age based on experimental data. Simulations were performed with three parameter sets corresponding to 20 years, 60 years and 100 years (interpolated) (supplementary information). The GE response curves were interpolated for the ages in between.

Individualized GEC predictions

Personalized GEC is calculated by combining a predictor for liver volumes and blood flow from anthropomorphic information (age, body weight, height, BSA) with the multiscale model galactose elimination curves (GE), allowing the calculation of age-dependent GEC for given perfusion in volume of liver tissue.

The dependencies between liver volume/blood flow and anthropomorphic features are described via generalized additive models for location, scale and shape (GAMLSS) {Stasinopoulos2007} fitted to individual data from >3000 subjects from >30 studies (supplement GAMLSS). The resulting models enable the prediction of probability distributions of liver features for given anthropomorphic features, e.g. the distribution of liver volumes

depending on age, body weight or height. In a second step, the prediction of liver volume for a set of anthropomorphic features is generated by combining the single feature models (assumption of statistical independence). The result is a personalized probability distribution of liver volumes p_k(volLiver) for the subject k with sex=S, age=A, bodyweight=B, height=H. Hepatic blood flows is calculated analogue, but integrates the additional correlation between liver volume and blood flow, resulting in a distribution of liver blood flows for given liver volumes and anthropomorphic features p_k(flowLiver|volLiver).

GEC for person k from total blood flow ($flowLiver_k$) and liver volume ($volLiver_k$) results as

$GEC_k = f_{GEC\_per\_volLiver,\ age=agek}(flowLiver_k/volLiver_k,\ gal=8mM) * volLiver_k$

Via repeated sampling from the individualized probability distributions pk(volLiver) and pk(flowLiver|volLiver) the distribution of liver volumes, blood flows and corresponding GEC is calculated.

Population variability

To calculate the population variability in liver function the prediction of liver volume, blood flow and GEC was performed for a large cohort representative of the US population. The NHANES {NHANES} survey data between years 1999 - 2012 was used, with subjects filtered based on body mass index ($18.5 \leq BMI \leq 24.9$) and ethnicity (Non-Hispanic White). For all subjects with complete data sets of age, gender, height, and body weight the prediction was performed. Using the Monte Carlo approach, repeated computations based on inputs selected at random from statistical distributions for each input parameter are conducted to provide a statistical distribution of the output. Using high percentile (e.g. 95th) and 50th percentile, the intraspecies variability can be calculated. To derive this information, Monte Carlo simulations based on distributions of input parameters have frequently be used. (Lipscomb et al., 2003; Gentry et al., 2002; Haber et al., 2002; Lipscomb and Kedderis, 2002; Timchalk et al., 2002; Bogaards et al., 2001; El-Masri et al., 1999; Thomas et al., 1996a, b).

Classification

The multiscale model classification of disease status is based on the standard deviation sd_{GEC} and the 5% quantile q_{GEC} of the distribution of predicted GEC values for given anthropomorphic features and the experimental GEC value

$$p_{multiscale} = \frac{q_{GEC} - GEC}{sd_{GEC}}$$

Performance of the classifier was evaluated against logistic regression with various predictors on identical datasets (corresponding to the maximal dataset containing values for all predictor variables necessary for the respective logistic regression model). Logistic regression performance was calculated via bootstrap model fitting (N_B=100). Fitting of logistic models was implemeted in R. AUC and ROC curves were calculated with R package ROCR. The multiscale model classifier was implemented as a web application in Shiny R.

FIGURES

Figure 1 *– Model overview of hepatic galactose metabolism on cellular, tissue- and organ-scale and application in prediction of individual galactose clearance*

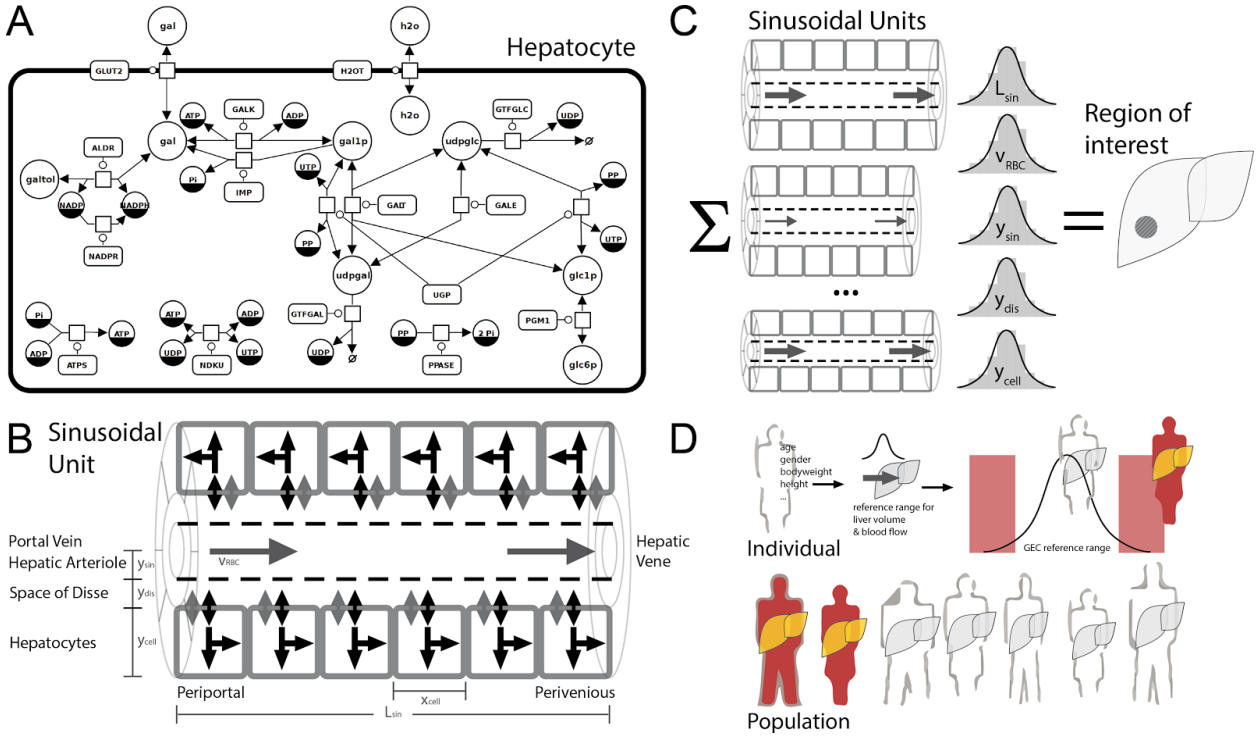

A) Overview of detailed kinetic model of hepatic galactose metabolism in SBGN {LeNovere2009}.
Reactions: (ALDR) **Aldose reductase (galactitol NAD 1-oxidoreductase);** (ATPS) **ATP synthesis;** (GALDH) **Galactose 1-dehydrogenase;** (GALE) **UDP-glucose 4-epimerase;** (GALK) **Galactokinase;** (GALT) **Galactose-1-phosphate uridyl transferase;** (GLUT2) **Facilitated glucose transporter member 2;** (GTFGAL) **Glycosyltransferase galactose;** (GTFGLC) **Glycosyltransferase glucose;** (NADPR) **NADP reductase;** (NDKU) **Nucleoside diphosphokinase, ATP:UDP phosphotransferase;** (IMP) **Inositol monophosphatase;** (PGM1) **Phosphoglucomutase-1;** (PPASE) **Pyrophosphatase;** (UGALP) **UDP-galactose pyrophosphorylase;** (UGP) **UDP-glucose pyrophosphorylase;**
Metabolites: (adp) **ADP;** (atp) **ATP;** (gal) **D-galactose;** (gal1p) **D-galactose 1-phosphate;** (galnat) **D-galactonate;** (galtol) **D-galactitol;** (glc) **D-glucose;** (glc1p) **D-glucose 1-phosphate;** (glc6p) **D-glucose 6-phosphate;** (nadp) **NADP;** (nadph) **NADPH;** (pi) **phosphate;** (pp) **pyrophosphate;** (udp) **UDP;** (udpgal) **UDP-D-galactose;** (udpglc) **UDP-D-glucose;** (utp) **UTP;**
B) Tissue-scale model of the sinusoidal unit comprising diffusion and convection based transport of substances in the sinusoid, diffusion-based transport of substances in the space of Disse and description of cellular metabolism via kinetic models of individual hepatocytes. Blood coming from the hepatic artery and portal vein enters the sinusoidal unit periportal and leaves pericentral. Transport between the sinusoid and the space of Disse occurs via fenestrations in the endothelial cells. Parameters and references are provided in the supplement.
C) Region of interests of the liver are modeled via the integration of multiple sinusoidal units based on the observed heterogeneity of structural parameters and microcirculation within the lobulus.

D) Based on anthropomorphic information of subjects like age, gender, bodyweight and height the region of interests are scaled to the observed distributions of liver blood flow and liver volume. Reference values of galactose clearance (GEC) are calculated and the experimental value of GEC can be evaluated in this reference context. Based on available data on the distribution of anthropomorphic features (NHANES {REF}) the population variability can be evaluated.

Figure 2 *– Parameter distributions and resulting multiple-indicator dilution curves*

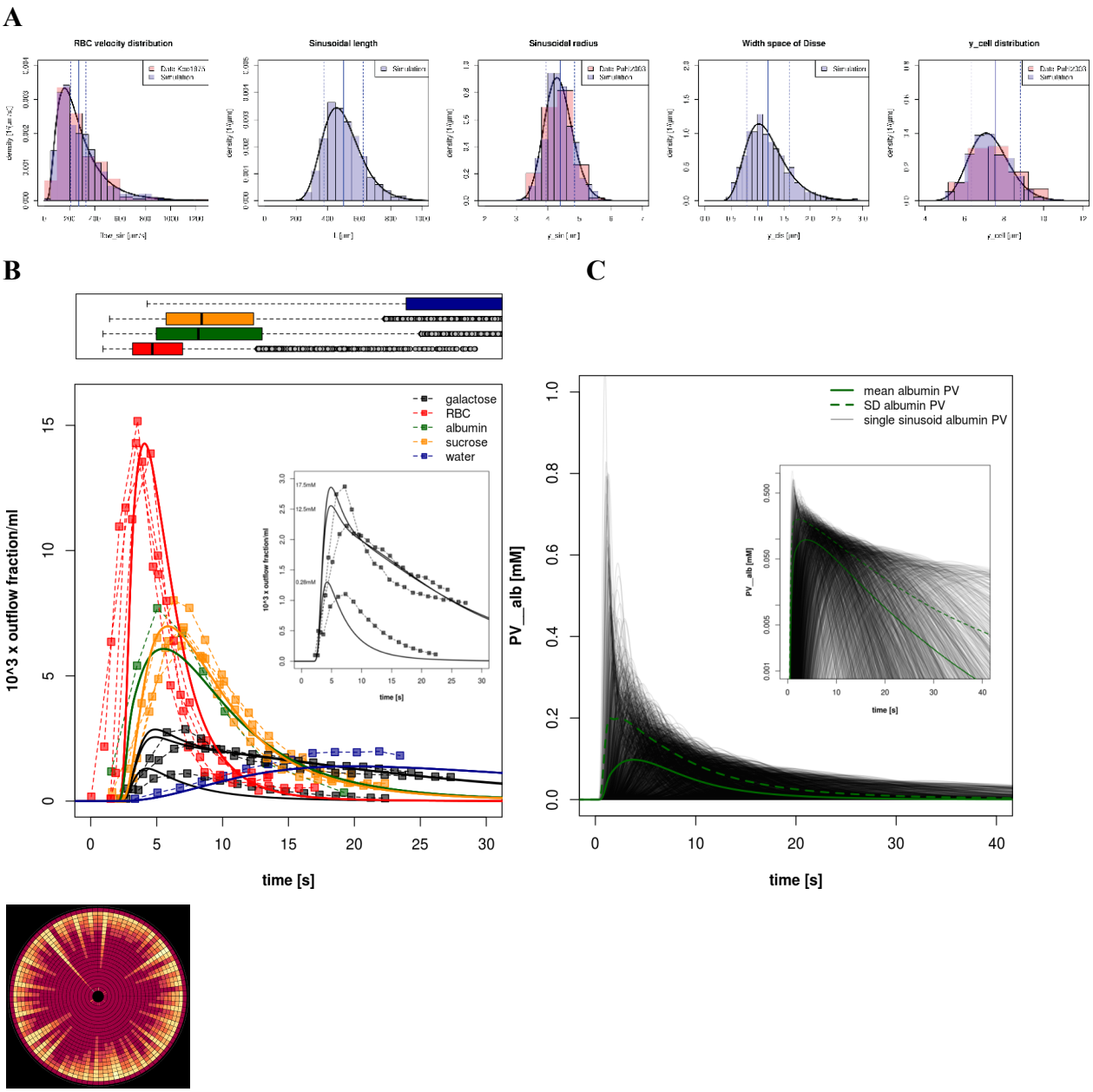

A) Experimental parameter distributions (see Supplementary Information for references) and distribution of parameter samples (N=2000) underlying calculation of multiple indicator dilution curves. To simulate the liver function of a region of interest the response of the samples of structural different sinusoidal units is integrated.

B) Resulting integrated multiple-indicator dilution curves of traced red blood cells (red), albumin (green), sucrose (orange), water (blue) and galactose (gal) after a rectangular tracer peak of duration 0.5s (see inlet) with experimental data from {Goresky1973, Goresky1983}. Three simulations corresponding to the experimental conditions of varying unlabeled galactose concentrations of 0.28mM, 12.5mM and 17.5mM are depicted. Inlet shows the multiple-indicator dilution curves of traced galactose corresponding to B. An increase in unlabeled galactose results in competitive inhibition of galactose transport into the liver.

C) Perivenous albumin concentrations of single sinusoids. Individual curves for the sampled geometries with mean (solid) and mean+-std (dashed). The response of the different sinusoids is very heterogenous and the actual dilution behavior depends strongly on the local microarchitecture.

Figure 3 *– Sinusoidal gradients in galactose metabolization*

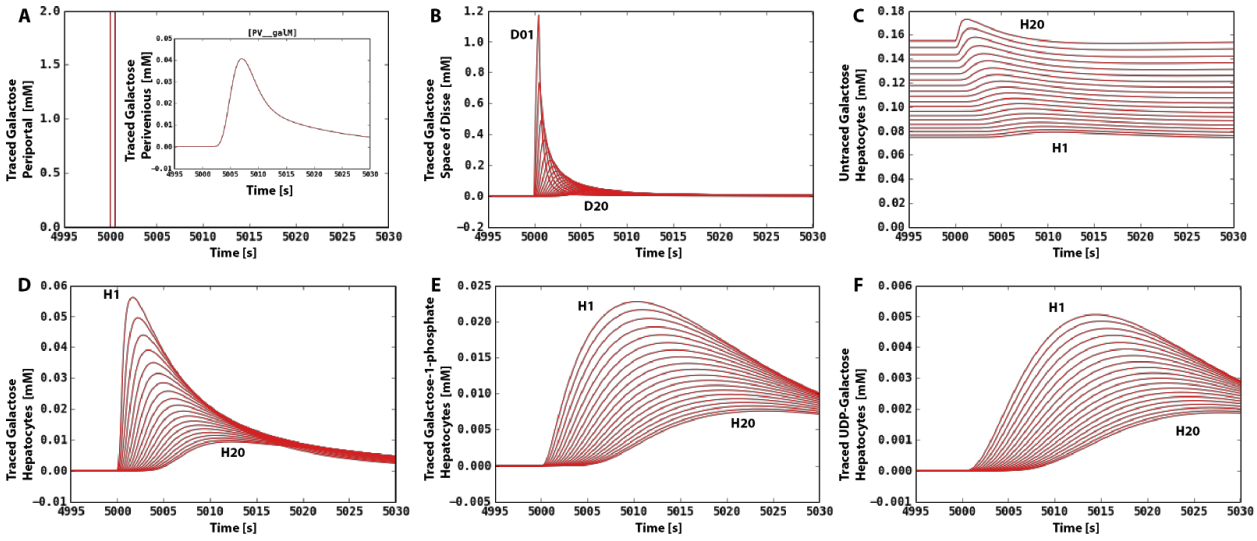

Sinusoidal gradients in galactose metabolism after traced galactose is given. Periportal traced galactose under constant untraced galactose load of 0.28mM (corresponding to lowest galactose concentration in figure 2). Simulation of a single sinusoidal unit (mean sinusoidal unit with mean structural and flow parameters) is shown.

A) Applied periportal galactose tracer (rectangular peak of duration 0.5s). Tracer is given at t=5000s after system reached steady state under the untraced galactose load. Resulting perivenous traced galactose concentration is depicted in the inlet.

B) Concentration of traced galactose in the space of Disse (Space of Disse adjacent to the first periportal hepatocyte H01 is D01, adjacent to the last perivenous hepatocyte H20 is D20.

C) Untraced galactose concentration in hepatocyte H01 (periportal) to H20 (perivenous). Untraced galactose increases in the hepatocytes along the sinusoids due to the competitive inhibition (alternative substrate) of Galactokinase via the traced galactose in the hepatocytes.

D) Traced galactose in hepatocytes along the sinusoid.

E) Traced galactose-1 phosphate in hepatocytes along the sinusoid. Galactokinase is the rate limiting step.

F) Traced UDP-galactose concentration in the hepatocytes along the sinusoid.

Figure 4 *– Hepatic galactose elimination, extraction ratio, and flow-dependent clearance and extraction ratio on tissue scale & the effect of aging (A-H) & Whole liver galactose elimination, extraction ratio, and clearance (I-O).*

A-H

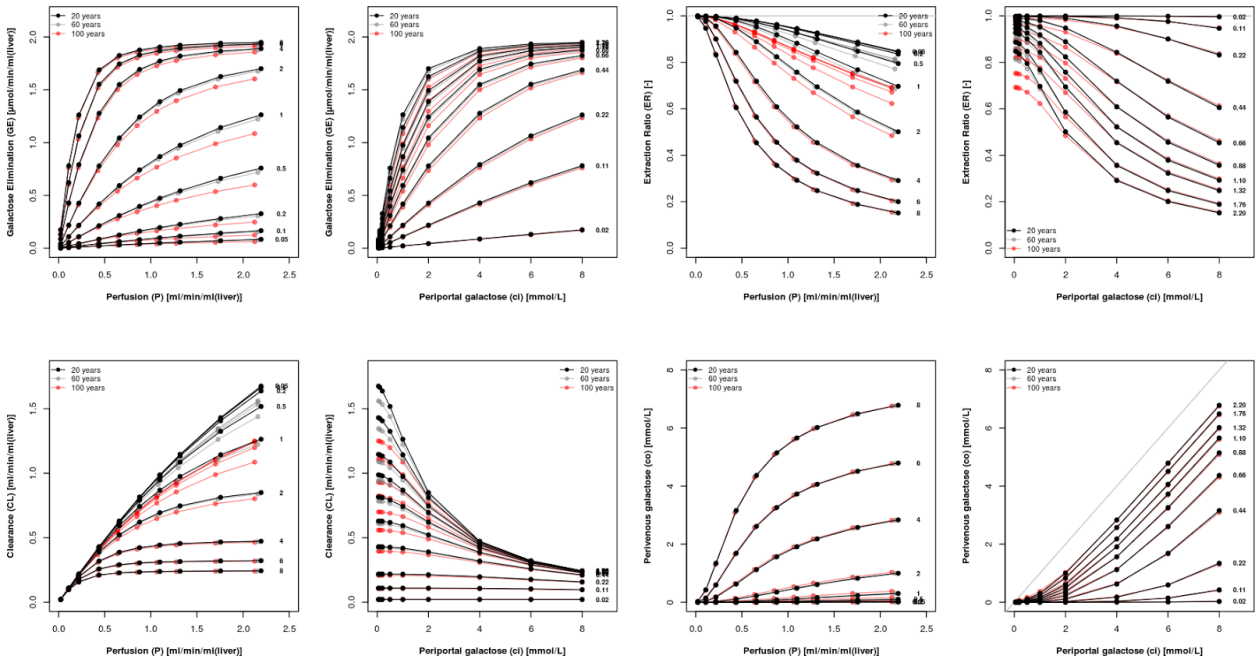

I-O

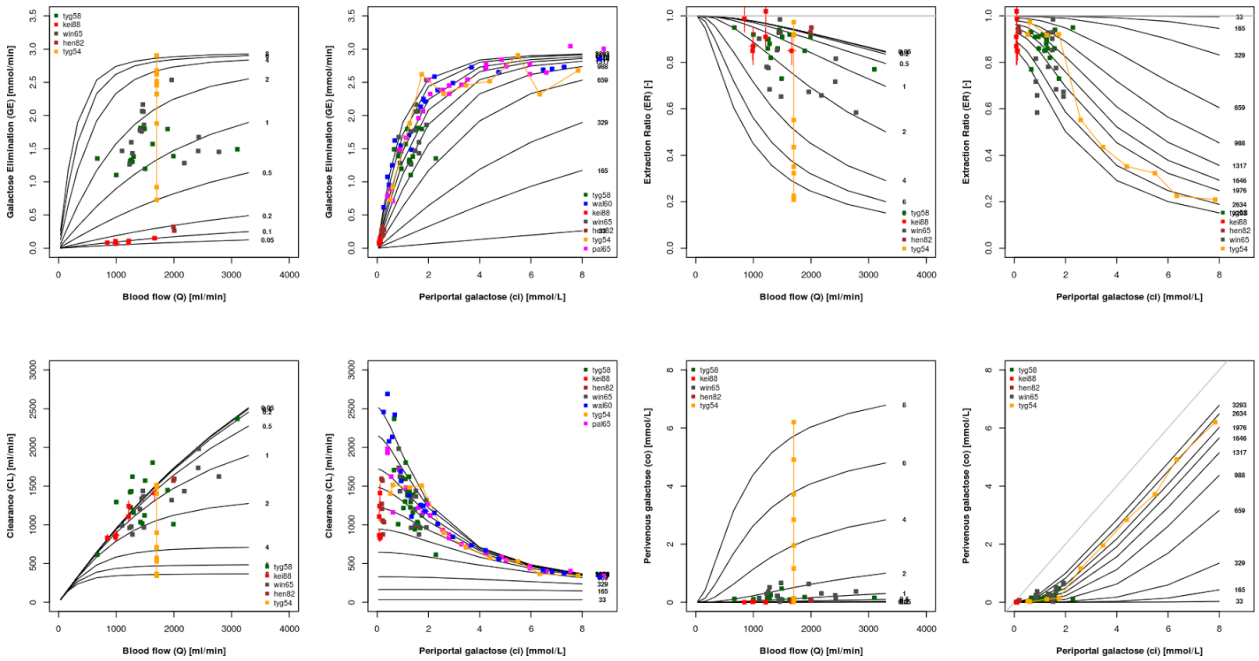

Steady state galactose elimination (GE), Clearance (CL), Extraction Ratio (ER) and perivenous galactose concentration (co) depending on blood flow and periportal galactose concentration (ci) and age dependent changes in ultrastructure (pseudocapillarization).

Curves for unaltered ultrastructure (corresponding to age of 20 years) in blue and advanced pseudocapillarization via defenestraetion and widening of endothelial cells (corresponding to age 100 years) in red. Every data point is the integration over N=100 simulations based on samples from the underlying ultrastructure and perfusion to steady state under the given conditions.

I-O Comparison of predictions with individual subject data in human {Keiding1988, Tygstrup1958, Tygstrup1954, Waldstein1960, Henderson1982, Winkler1965, Palu1965}

Figure 5 *– Organ heterogeneity in galactose elimination, extraction ratio, and clearance. Integration under perfusion heterogeneity of normal subjects.*

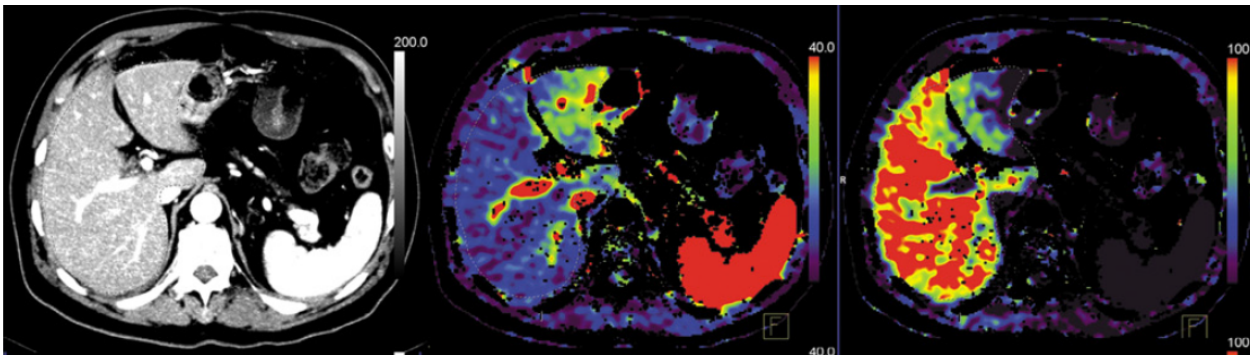

Figure 6 *– Individualized GEC prediction, prediction of population variability & age dependence and successful classification of liver disease*

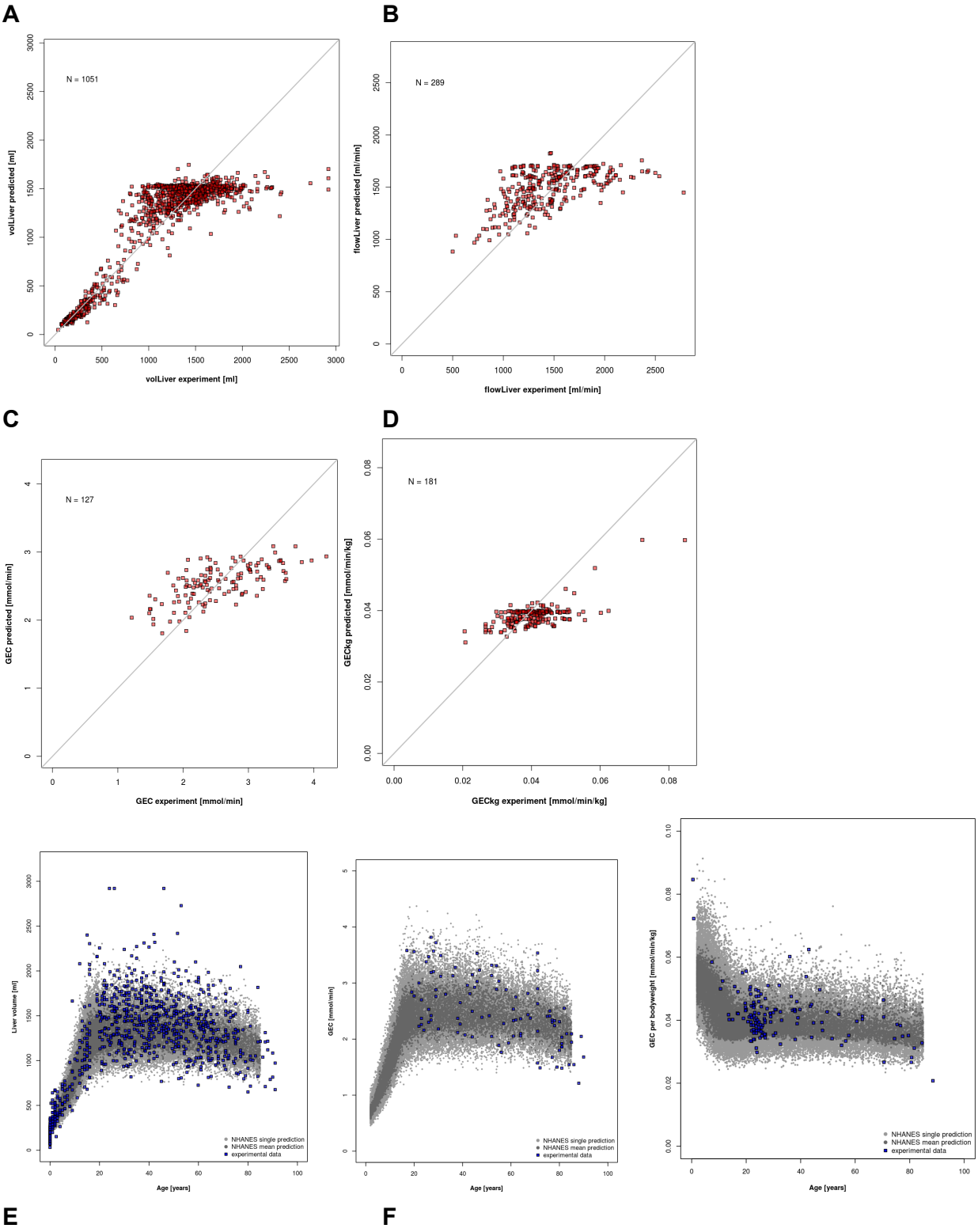

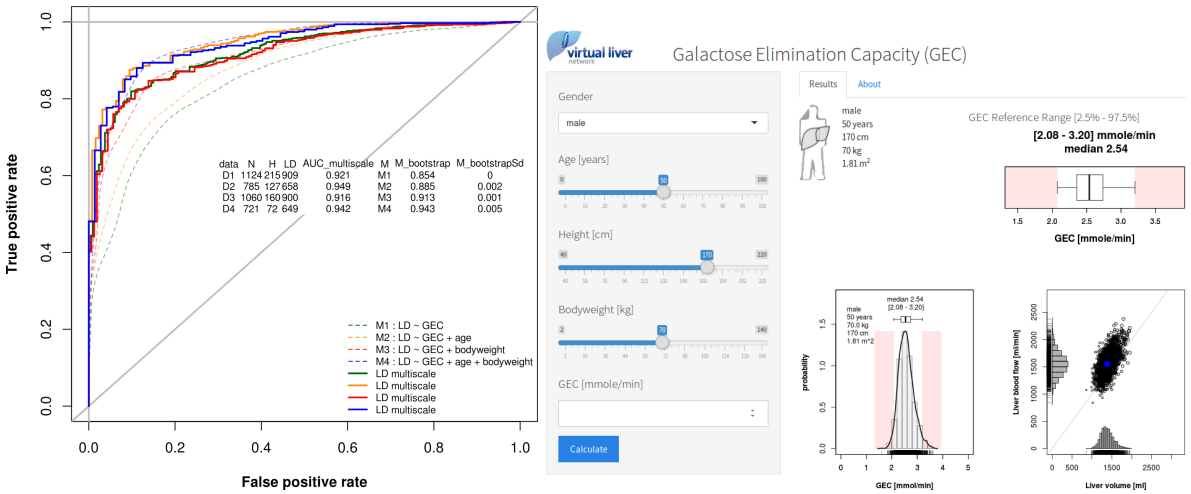

A) Prediction of normal GEC range based on the subset of available anthropomorphic information. Comparison with experimental data.
B) Prediction of normal GEC per bodyweight based on the subset of available anthropomorphic information. Comparison with experimental data (large subset of the data is independent from A, thereby providing independent validation of method.
C) Predicted population variability of GEC in healthy subjects based on the anthropomorphic infromation available in the NHANES cohort. Available experimental GEC data shown in comparison.
D) Predicted GEC per bodyweight population variability from NHANES cohort. Available experimental GEC dta shown in comparison. Large subset of GEC per bodyweight data is independent from C, providing independent validation of method.

E) Performance evaluation of individualized GEC classifier for liver disease. The multiscale classifier was compared to a series of logistic regression models using varying predictor variables. An overview about the various data subsets and the resulting areas under the curve (AUC) for the various models is given in the figure.
G) Screenshot of the web based application for prediction of GEC ranges and liver disease based on GEC measurements available at https://www.livermetabolism.com/gec_app/.